Shielding effects in fusion reactions with a proton-halo nucleus*

Xue-ying He(何雪英)[1,2] Qin Dong(董琴)[1,2] Li Ou(欧立)[1,2;1)]

[1]College of Physics and Technology, Guangxi Normal University, Guilin 541004, China
[2]Guangxi Key Laboratory of Nuclear Physics and Technology, Guangxi Normal University, Guilin 541004, China

Abstract: To explain the experimental observation that the fusion cross-section of a proton-halo nucleus with a heavy target nucleus is not enhanced as expected, the shielding hypothesis was proposed, where the proton-halo nucleus is polarized and the valence proton shielded by the core. In the frame of the improved quantum molecular dynamics model, the fusion reaction ^{17}F on ^{208}Pb around the Coulomb barrier is simulated. The existence of the shielding effect is verified by the microscopic dynamics simulations. Its influence on the effective interaction potential is also investigated.

Keywords: halo nucleus, fusion reaction, shielding effect

DOI: 10.1088/1674-1137/44/5/054108

1 Introduction

Heavy-ion fusion reactions have attracted much attention in recent years [1-4], because they are not only one of the important ways to synthesize new super-heavy elements (SHE), but also an important method to study nuclear structure and nuclear reaction mechanisms. With rare radioactive beams provided by many laboratories in the world, it is possible to study the properties of nuclei located near the drip lines, and to study nuclear reactions by using projectiles with exotic properties, considerably different from those along the β stability line. Because of new phenomena in weakly bound nuclei [5-12], such as increased probability of neutron transfer and fusion [13] and increased breakup probability, one of the hot topics in SHE synthesis is the fusion with weakly bound nuclei, especially with halo nuclei.

Halo nuclei, in which the valence neutron(s) or proton(s) are very weakly bound, are expected to give rise to new phenomena in nuclear reactions. In the semiclassical picture, the nucleus with a low binding energy usually has a larger radius, and the probabilities of specific reaction channels, such as neutron transfer and fusion, increase [13]. However, the experiments with the proton drip line nucleus ^{17}F on ^{208}Pb at energies around the Coulomb barrier do not observe enhancement of the fusion cross-section due to breakup or to the large interaction radius [14]. For the reaction ^{17}F+^{208}Pb at energies around the Coulomb barrier, Liang showed that the influence of breakup of ^{17}F on the fusion cross-section is quite weak [5]. One of the hypothesis to explain the experimental data is the so-called "shielding effect". In the reaction, ^{17}F is excited to the first excited state, becomes a proton-halo nucleus (hereafter denoted as ^{17}F*), and is polarized as the valence proton is repelled by the reaction partner, and is shielded by the ^{16}O core. With such a shielding effect, the effective interaction radius is smaller than one of ^{17}F in the first excited state, and the fusion rate does not increase as expected.

In this work, using the improved quantum molecular dynamics model (ImQMD) and taking ^{17}F+ ^{208}Pb as an example, we try to verify the existence of the shielding effect of the valence proton in fusion reactions, and investigate its influence on the effective interaction potential. The paper is organized as follows. In Sec. 2, we briefly introduce the model. In Sec. 3, we present the improvement of the ImQMD model needed to describe the halo nucleus and the shielding effect in fusion reactions. Finally, a brief summary is given in Sec. 4.

2 The model

The quantum molecular dynamics (QMD) model built by Aichelin and Peilert et al. [15, 16], which intuitively

Received 21 November 2019, Revised 18 January 2020, Published online 18 March 2020

* Supported by National Natural Science Foundation of China (11965004, U1867212, 11711540016, 11847317, 11947413), Natural Science Foundation of Guangxi province (2016GXNSFFA380001, 2017GXNSFGA198001), Foundation of Guangxi innovative team and distinguished scholar in institutions of higher education, and Innovation project of Guangxi Graduate Education (XYCSZ2018051)

1) E-mail: liou@gxnu.edu.cn

describes the microscopic dynamics of a nuclear reaction, is a powerful tool for studying heavy-ion collisions (HICs) at intermediate energies. Several versions of the QMD model, such as ImQMD, IQMD, IQMD-BNU, IQMD-IMP, IQMD-SINAP, JAM, JQMD, TuQMD, UrQMD, have been developed and successfully applied in various research fields. A detailed discussion of the QMD models can be found in Refs. [17-19]. The ImQMD model [20-26], used in this work, is briefly described below.

In the ImQMD model, the nucleon is represented by a Gaussian wave packet, which reads

$$\phi_i(\boldsymbol{r}) = \frac{1}{(2\pi\sigma_r^2)^{3/4}} \exp\left[-\frac{(\boldsymbol{r}-\boldsymbol{r}_i)^2}{4\sigma_r^2} + \frac{i}{\hbar}\boldsymbol{r}\cdot\boldsymbol{p}_i\right], \tag{1}$$

where $\boldsymbol{r}_i$, $\boldsymbol{p}_i$ is the center of the wave packet of the ith nucleon in the coordinate and momentum spaces, and σ_r is the width of the wave packet in the coordinate space. Considering the size of the system, σ_r can be expressed as

$$\sigma_r = \sigma_0 A^{1/3} + \sigma_1, \tag{2}$$

where A is the nucleon number, and σ_0 and σ_1 are the parameters obtained by fitting the properties of many β stable nuclei. Using the Wigner transform of the nucleon wave function and summing over all nucleons, one can get the phase space distribution function of the nuclear system, which reads

$$f(\boldsymbol{r},\boldsymbol{p}) = \sum_i^A f_i(\boldsymbol{r},\boldsymbol{p}) = \sum_{i=1}^A \frac{1}{(\pi\hbar)^3} \exp\left[-\frac{(\boldsymbol{r}-\boldsymbol{r}_i)^2}{2\sigma_r^2}\right] \times \exp\left[-\frac{(\boldsymbol{p}-\boldsymbol{p}_i)^2}{2\sigma_p^2}\right], \tag{3}$$

where σ_p is the width of the wave packet in the momentum space, which satisfies the minimum uncertainty relation $\sigma_r \cdot \sigma_p = \frac{\hbar}{2}$. The center of the wave packet for each nucleon evolves following the Hamilton canonical equations,

$$\dot{\boldsymbol{r}}_i = \frac{\partial H}{\partial \boldsymbol{p}_i}, \quad \dot{\boldsymbol{p}}_i = -\frac{\partial H}{\partial \boldsymbol{r}_i}. \tag{4}$$

The Hamiltonian, including the kinetic energy, Coulomb energy and nuclear local potential energy, reads

$$H = T + U_{\rm Coul} + U_{\rm loc}. \tag{5}$$

Each term of the Hamiltonian is written as

$$T = \sum_i^A \frac{p_i^2}{2m}, \tag{6}$$

$$U_{\rm Coul} = \frac{1}{2}\int \rho_p(\boldsymbol{r})\frac{e^2}{|\boldsymbol{r}-\boldsymbol{r}'|}\rho_p(\boldsymbol{r}')\mathrm{d}\boldsymbol{r}\mathrm{d}\boldsymbol{r}', \tag{7}$$

$$U_{\rm loc} = \int V_{\rm loc}\mathrm{d}\boldsymbol{r}, \tag{8}$$

where $V_{\rm loc}$ is the Skyrme potential energy density functional without the spin-orbit term, which can be expressed as

$$V_{\rm loc} = \frac{\alpha}{2}\frac{\rho^2}{\rho_0} + \frac{\beta}{\gamma+1}\frac{\rho^{\gamma+1}}{\rho_0^{\gamma}} + \frac{g_{\rm sur}}{2}(\nabla\rho)^2 + g_\tau\frac{\rho^{\eta+1}}{\rho_0^{\eta}} + \frac{C_{\rm s}}{2\rho_0}[\rho^2 - \kappa_{\rm s}(\nabla\rho)^2]\delta^2. \tag{9}$$

Here, ρ and ρ_0 are the nucleon density and the saturation density, respectively, and $\delta = (\rho_n - \rho_p)/\rho$ is the isospin asymmetry. The parameter set used in Eq. (9), called IQ3a, which has been successfully applied to the study of fusion reactions [27, 28], is listed in Table 1.

3 Results and discussion

3.1 Preparation of the halo nucleus

The first step to simulate the reaction with the ImQMD model is the initialization of the projectile and target nuclei. As is well known, a good initial nucleus is very important for QMD calculations, especially for reactions at low energies. A typical method for preparing the initial nucleus in QMD is the following: first, the position of each nucleon is determined by Monte Carlo sampling according to the size of the nucleus. Second, based on the density distribution

$$\rho(\boldsymbol{r}) = \int f(\boldsymbol{r},\boldsymbol{p})\mathrm{d}\boldsymbol{p} = \frac{1}{(2\pi\sigma_r^2)^{3/2}}\sum_{i=1}^A \exp\left[-\frac{(\boldsymbol{r}-\boldsymbol{r}_i)^2}{2\sigma_r^2}\right], \tag{10}$$

the local Fermi momentum is obtained in the local density approximation $P_F = (\frac{3\pi^2}{2}\rho)^{1/3} - \Delta p_F$, where ΔP_F is the contribution of the width of the wave packet and is determined by the binding energy. The initial momentum of each nucleon is sampled randomly in the range 0-P_F. To check the stability of the prepared nucleus, the prepared nuclear system is evolved on its own for a short or long period of time, depending on the type of reaction. Only those nuclei with satisfactory properties, such as the root-mean-square (rms) radius, binding energy, and time evolution, and for which there is no spurious particle emission for a sufficiently long time, are selected as "good initial nuclei".

In order to describe the halo-nucleus, which is a weakly bound nucleus, with such a semi-classical model, special treatment in ImQMD must be used. The halo-nucleus is usually considered as a system with a loose

Table 1. The model parameter set IQ3a.

α/MeV	β/MeV	γ	$g_{\rm sur}$/(MeV fm^2)	g_τ/MeV	η	$C_{\rm s}$/MeV	$\kappa_{\rm s}$/fm^2	ρ_0/fm^{-3}	σ_0/fm	σ_1/fm
−207	138	7/6	16.5	14.0	5/3	34.0	0.4	0.165	0.02	0.94

valence nucleon moving around a tight core. Taking the proton-halo nucleus $^{17}F^{*}$, its rms radius is 2.71 ± 0.18 fm, and the rms radius of the valence proton is 5.33 fm [29-31]. Hence, $^{17}F^{*}$ is considered as a system with a ^{16}O core and a valence proton. To save CPU time in ImQMD calculations, the initial distance between the projectile and the target is not infinity, as in the real situation, but has a finite value of 40 fm. There is a very large probability for ^{17}F to be excited by the heavy target nucleus at such a short distance. Therefore, we sample the $^{17}F^{*}$ nuclei in the initial state. In the ImQMD model, the ^{16}O core is prepared by the standard method. The experimental value of the rms radius of the neutron in the first excited state of $^{17}F^{*}$ is 2.478 fm, meaning that the ^{16}O core of $^{17}F^{*}$ is smaller than the ordinary ^{16}O nucleus, which has an rms radius of 2.710 fm. As a result, the radius and the wave packet width calculated using the ordinary ^{16}O, are both multiplied by 0.9 in the sampling of the ^{16}O core. In order to set the valence proton with reasonable properties, two factors are considered. One is the position of the valence proton, which should be far away from the core in order to form the halo. The other is the wave packet width of the valence proton, which reflects the range of the nuclear force and has a clear effect on nucleus surface diffusion [32]. It is obvious that Eq. (2) for the wave packet width of the ordinary nucleon is not suitable for the loosely bound valence proton. The extreme surface diffusion structure of $^{17}F^{*}$, i.e. its halo, requires a relatively large width of the valence proton wave packet. By optimally fitting the experimental data for $^{17}F^{*}$, the initial distance between the valence proton and the center-of-mass of the core is set to $R = R_{\rm p} + 1.6$ fm, where $R_{\rm p}$ is the radius of the proton distribution of the ^{16}O core [33, 34]. The wave packet width and the initial momentum is set to $\sqrt{2}$ fm and 25 MeV/c, respectively.

The ImQMD model is a semiclassical model with the Skyrme δ-type interaction. It is quite difficult for a weakly bound nucleus, such as a halo nucleus, to be stable for a long time in this kind of model. The valence proton will finally fall into the core due to its strong attraction. To maintain a stable halo, the so-called "sphere-shell constraint" is introduced into the model. If the valence proton is too close to the core and tends to move towards the core, or if it is too far and tends to move back to the core, its momentum direction is changed randomly by elastic scattering with the nucleon nearby.

Modifications of the method of preparing the initial nucleus and the introduction of the sphere-shell constraint, allow to get $^{17}F^{*}$ which has sufficiently good properties and is stable enough. In Fig. 1, the density distributions of the nucleons, protons, neutrons and the valence protons in $^{17}F^{*}$ at 0 and 1000 fm/c are shown. The experimental data [30] and the relativistic density dependent Hartree theory (RDDH) [30, 35], are also shown for comparison. It can be seen that although the halo of the initial $^{17}F^{*}$ is small, the distributions given by the ImQMD model are reasonable. As the nucleons self-adjust with time, the ImQMD model gives quite a good distribution, close to the experimental results and the RDDH theory.

In Fig. 2 , we show the time evolution of the deviation of the binding energy and of the rms radii of nucle-

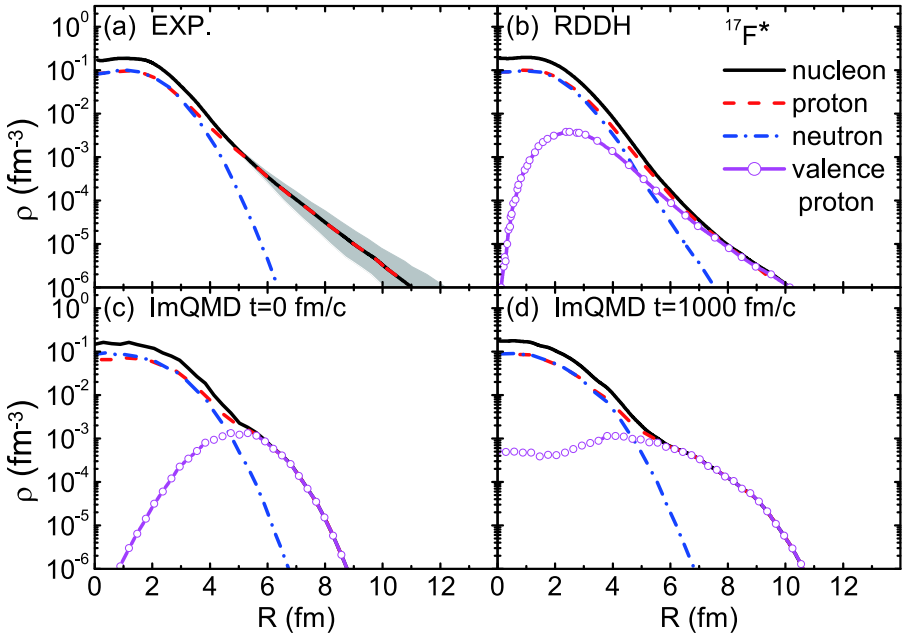

Fig. 1. (color online) Density distributions of the nucleons, protons, neutrons and the valence protons in $^{17}F^{*}$ from experiments (a), relativistic density dependent Hartree(RDDH) theory (b), and the ImQMD calculations (c) (d).

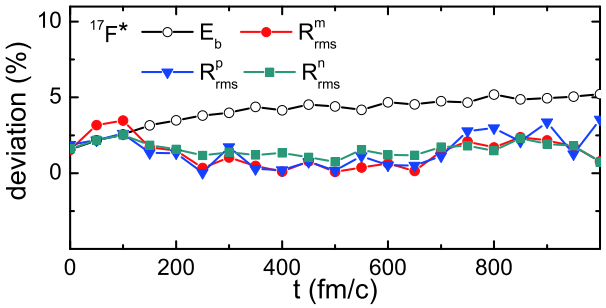

Fig. 2. (color online) Time evolution of the deviation of the binding energy and of the rms radii of nucleons, protons and neutrons in ^{17}F*.

ons, protons, and neutrons in ^{17}F*. The binding energy and the rms radii remain stable, with small fluctuations, for a sufficiently long time.

3.2 Proton-halo nucleus fusion reaction

To obtain a stable halo structure, the sphere-shell constraint, which is not a self-consistent treatment, was introduced into the model. The halo structure is easily destroyed when the halo nucleus enters the field of the target nucleus. Hence, the sphere-shell constraint should be switched off at a proper moment in the simulation, and the valence proton can then move self-consistently in the field of the system. To select a proper switch-off time, the time evolution of the ratio between the force on the valence proton from ^{208}Pb and from the core ^{16}O was investigated, shown in Fig. 3 by the solid curve. For comparison, we also calculated the ratio between the Coulomb force on the valence proton from ^{208}Pb and from the core ^{16}O, shown by the dashed curve, assuming that the projectile and target are two charged points located at their individual center-of-mass, and that they move with their initial velocities. One can see that at the early stage, the effect from the target is quite weak and that the Coulomb force dominates. The influence of the target becomes rapidly stronger from 150 fm/c, and the effect of the nuclear force becomes obvious. Therefore, the sphere-shell constraint is switched off at 150 fm/c in the following calculations.

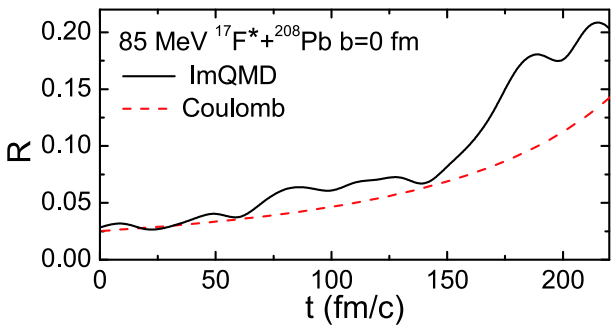

Fig. 3. (color online) Time evolution of the ratio between the force on the valence proton from ^{208}Pb and from the core of ^{17}F*.

We first checked the shielding of the valence proton by the ^{16}O core in the reaction ^{17}F*+^{208}Pb at the energy $E_{\rm c.m.}$ = 85 MeV and b = 0 fm. As illustrated in Fig. 4, the angle θ between the position vector of the valence proton and the center-of-mass of ^{16}O could be a criterion for shielding. If $\cos\theta < 0$, the valence proton is considered to be shielded by the ^{16}O core.

The proportion of valence protons which are shielded is defined as the ratio $N_{\rm s}/N_{\rm t}$, which is shown in Fig. 5. $N_{\rm s}$ and $N_{\rm t}$ are the number of events in which the valence proton is shielded during the reaction and the total number of events, respectively. The case for the individual ^{17}F* is also shown for reference. One can see that for the individual ^{17}F*, the valence proton is distributed uniformly in the halo. In the early stage of the ^{17}F*+^{208}Pb reaction, when the projectile is far from the target, there is no obvious shielding effect. As the projectile moves closer to the target, the shielded proportion increases. From 500 fm/c, there are more events with the valence proton shielded by the core. After 700 fm/c, when ^{16}O is absorbed by the target to form the compound nucleus or is elastically scattered, the shielding effect is disturbed.

By generating a large number of events at each incident energy $E_{\rm c.m.}$ and each impact parameter b and counting the number of fusion events, the fusion probability $g_{\rm fus}(E_{\rm c.m.}, b)$ can be obtained and the corresponding fusion cross-section calculated as

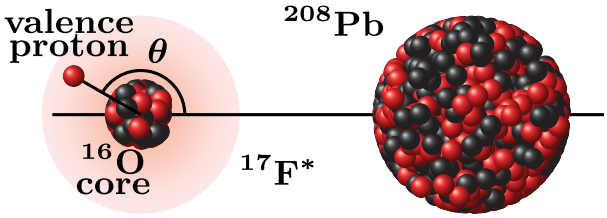

Fig. 4. (color online) Sketch of the valence proton shielded by the core.

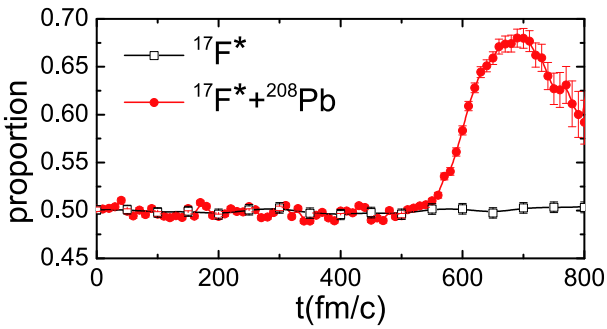

Fig. 5. (color online) Time evolution of the proportion of events in which the valence proton is shielded by the core.

$$\sigma_{\rm fus}(E_{\rm c.m.}) = 2\pi \int g_{\rm fus}(E_{\rm c.m.}, b) b {\rm d}b$$
$$\simeq 2\pi \sum g_{\rm fus}(E_{\rm c.m.}, b_i) b_i \Delta b, \quad (11)$$

where Δb = 1 fm. An event is counted as a fusion (capture) event if the center-to-center distance between the two nuclei is smaller than the nuclear radius of the compound nuclei. Here, the quasi-fission probability for the considered reaction systems is neglected [27].

In Fig. 6, we show the fusion excitation functions of ^{17}F*+^{208}Pb and ^{16}O+^{208}Pb calculated by the ImQMD model. The experimental data are shown for comparison. The results for ^{16}O+^{208}Pb are shifted in energy by the factor 9/8 (the ratio of charges of F and O). The fusion cross-section around and above the Coulomb barrier is reproduced quite well. Below the Coulomb barrier, the fusion cross-section of ^{17}F*+^{208}Pb is slightly higher than of ^{16}O+^{208}Pb, but both overestimate the experimental data, which is probably due to the fact that many quantum effects, such as the shell effect and the tunneling effect, cannot be simulated in the present semi-classical ImQMD model. Although the present version of ImQMD cannot describe fusion reactions at very low energies, it is still reasonable to investigate the shielding effect by comparing the fusion cross-sections of ^{17}F*+^{208}Pb and ^{16}O+^{208}Pb. From Fig. 6, one can see that the fusion cross-sections of ^{17}F*+^{208}Pb and ^{16}O+^{208}Pb are close to each other, with no enhancement above or below the Coulomb barrier.

As is well known, the classical fusion cross-section is $\sigma_{\rm fus} = \pi R_{\rm eff}^2$, where $R_{\rm eff}$ is the effective interaction radius which is directly related to the radii of the projectile and target. The system with a larger projectile and target nuclei will have a larger fusion cross-section. The rms radii of ^{17}F and ^{16}O are similar in the ground state. Once ^{17}F is excited by ^{208}Pb to a proton-halo nucleus with a larger radius, the fusion cross-section should be enhanced compared to ^{16}O+^{208}Pb. However, the enhancement is not observed in experiments. Taking the shielding effect into consideration, the valence proton is pushed toward or even behind the ^{16}O core, and the thickness of the halo facing the target becomes smaller. This effect reduces the effective interaction radius and changes the effective interaction potential between the projectile and target nuclei. In Fig. 7, we show the effective interaction potential for the fusion reaction ^{17}F*+^{208}Pb at the energy $E_{\rm c.m.}$ = 85 MeV and b = 0 fm, for the valence proton distributed uniformly, and for two extreme cases, the valence proton located in front of the ^{16}O core ($\theta = 0$) and totally shielded ($\theta = \pi$). One can see that before the projectile touches the target, the effective interaction potential is larger for $\theta = 0$ than for $\theta = \pi$, while after the projectile touches the target, the effective interaction potential is larger for $\theta = \pi$ than for $\theta = 0$. The competition between effective shielding and no shielding of the valence proton may be one of the possible reasons why the enhancement of the fusion cross-section is not observed. The result for ^{16}O+^{208}Pb at the energy $E_{\rm c.m.}$ = 76 MeV and b = 0 fm is also shown in the figure, shifted in energy by the factor 9/8. The similarity of the effective interaction potentials of ^{17}F*+^{208}Pb and ^{16}O+^{208}Pb indicates that these two systems essentially have the same behavior, as indicated by the fusion excitation functions.

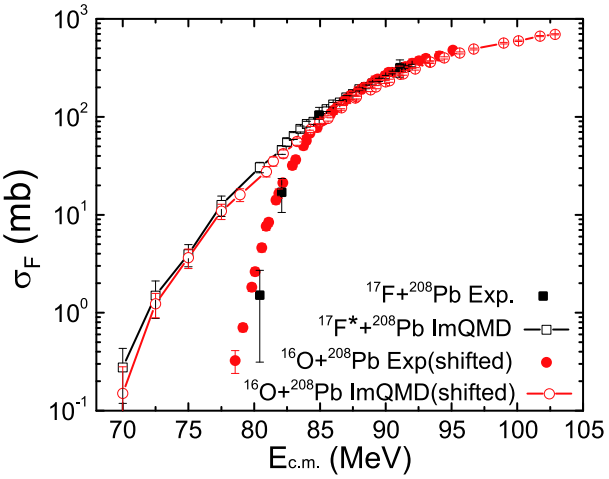

Fig. 6. (color online) Fusion excitation functions of ^{17}F*+^{208}Pb and ^{16}O+^{208}Pb calculated by the ImQMD model and compared to the experimental data. The results of ^{16}O+^{208}Pb are shifted in energy by the factor 9/8.

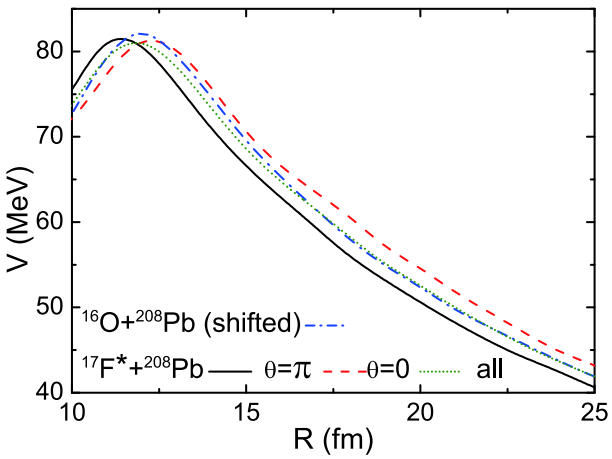

Fig. 7. (color online) Effective interaction potential for the fusion reactions ^{17}F*+^{208}Pb at the energy $E_{\rm c.m.}$ = 85 MeV and b = 0 fm, and ^{16}O+^{208}Pb at the energy $E_{\rm c.m.}$ = 76 MeV and b = 0 fm.

4 Summary

Experiments have shown that the fusion cross-section of a proton-halo nucleus with a heavy target nucleus is not enhanced compared to the regular nucleus as was expected. A reasonable hypothesis is that the valence proton moves away from the target nucleus and is shielded by the core of the halo nucleus, which is the so-called shielding effect. In this work, this effect was verified in fusion reactions by using the ImQMD model. To obtain satisfactory initial proton-halo nucleus, a special sampling method of the initial nucleus was introduced in ImQMD. The shielding phenomenon was verified in the reaction $^{17}F^{*}+^{208}Pb$ by tracing the relative position of the valence proton with respect to the core ^{16}O in microscopic dynamics simulations. The probability of shielding of the valence proton increases when the projectile and target get closer together. It is found that before the projectile and target touch, the shielding effect reduces the effective interaction potential, while after they touch, the shielding effect increases the effective interaction potential. The fact that the effective interaction potentials for $^{17}F+^{208}Pb$ and $^{16}O+^{208}Pb$ are similar leads to similar fusion excitation functions of these two systems.

The authors thank Dr. Ning Wang for careful reading of the manuscript and valuable discussions.

References

1 S. Hofmann and G. Munzenberg, Rev. Mod. Phys., **72**: 733 (2000)
2 Yu. Ts. Oganessian *et al*., Phys. Rev. Lett., **104**: 142502 (2010)
3 G. G. Adamian, N. V. Antonenko, A. Diaz-Torres *et al*., Nucl. Phys. A, **671**: 233 (2000)
4 B. N. Lu, E. G. Zhao, and S. G. Zhou, Phys. Rev. C, **85**: 011301(R) (2012)
5 J. F. Liang, J. R. Beenea, H. Esbensen *et al*., Phys. Lett. B, **491**: 23 (2000)
6 Z. H. Liu, M. Ruan, Y. L. Zhao *et al*., Phys. Rev. C, **69**: 034326 (2004)
7 N. Takigawa, M. Kuratani, and H. Sagawa, Phys. Rev. C, **47**: 2470R (1993)
8 M. S. Hussein, M. P. Pato, L. F. Canto *et al*., Phys. Rev. C, **47**: 2398 (1993)
9 C. Dasso, J. Guisado, S. Lenzi *et al*., Nucl. Phys. A, **597**: 473 (1996)
10 K. Hagino, A. Vitturi, C. H. Dasso *et al*., Phys. Rev. C, **61**: 037602 (2000)
11 A. M. Vinodkumar, W. Loveland, R. Yanez *et al*., Phys. Rev. C, **87**: 044603 (2013)
12 C. Dasso and R. Donangelo, Phys. Lett. B, **276**: 1 (1992)
13 C. Signorini, Nucl. Phys. A, **616**: 262c (1997), and references therein
14 K. E. Rehm, H. Esbensen, C. L. Jiang *et al*., Phys. Rev. Lett., **81**: 3341 (1998)
15 J. Aichelin, G. Peilert, A. Bohnet *et al*., Phys. Rev. C, **37**: 2451 (1988)
16 J. Aichelin, Phys. Rep., **202**: 233 (1991)
17 Jun Xu, Prog. Part. Nucl. Phys., **106**: 312 (2019)
18 Ying-Xun Zhang, Yong-Jia Wang, Maria Colonna *et al*., Phy. Rev. C, **97**: 034625 (2018)
19 Jun Xu, Lie-Wen Chen, ManYee Betty Tsang *et al*., Phy. Rev. C, **93**: 044609 (2016)
20 N. Wang, Z. Li, and X. Wu, Phys. Rev. C, **65**: 064608 (2002)
21 Ning Wang, Zhuxia Li, Xizhen Wu *et al*., Phys. Rev. C, **69**: 034608 (2004)
22 Y. Zhang and Z. Li, Phys. Rev. C, **71**: 024604 (2005)
23 L. Ou, Z. Li, and X. Wu, Phys. Rev. C, **78**: 044609 (2008)
24 Li Ou, Zhigang Xiao, Han Yi *et al*., Phys. Rev. Lett., **115**: 212501 (2015)
25 Junlong Tian, Xizhen Wu, Kai Zhao *et al*., Phys. Rev. C, **77**: 064603 (2008)
26 Kai Zhao, Zhuxia Li, Xizhen Wu *et al*., Phys. Rev. C, **88**: 044605 (2013)
27 Ning Wang, Li Ou, Yingxun Zhang *et al*., Phys. Rev. C, **89**: 064601 (2014)
28 Ning Wang, Zhuxia Li, Kai Zhao *et al*., Mech. Astr., **58**: 112001 (2015)
29 R. Morlock, R. Kunz, A. Mayer *et al*., Phys. Rev. Lett., **79**: 3837 (1997)
30 H. Zhang, W. Shen, Z. Ren *et al*., Nucl. Phys. A, **707**: 303 (2002)
31 D. Tilley, H. Weller, and C. Cheves, Nucl. Phys. A, **564**: 1 (1993)
32 T. Maruyama, K. Niita, and A. Iwamoto, Phys. Rev. C, **53**: 297 (1996)
33 B. Nerlo-Pomorska and K. Pomorski, Zeitschrift für Physik A Hadrons and Nuclei, **348**: 169-172 (1994)
34 W. Myers and W. Światecki, Phys. Rev. C, **62**: 044610 (2000)
35 Z. Ren, A. Faessler, and A.Bobyk, Phys. Rev. C, **57**: 2752 (1998)